MEASUREMENT AND EVALUATION OF CLIFF-TOP TURBULENCE USING A RESEARCH HELICOPTER

Naoki Matayoshi Yoshinori Okuno
Japan Aerospace Exploration Agency
Mitaka, Tokyo, Japan

Norihisa Maeyama Pingtong Zeng
Japan Weather Association
Toshima, Tokyo, Japan

Yoshinori Kose Hirofumi Sato
Toho Air Service Co. LTD.
Chofu, Tokyo, Japan

Abstract

This paper describes the measurement and evaluation of cliff-top turbulence for a planned heliport qualification. Investigation of the local wind field included a numerical analysis using computational fluid dynamics (CFD) conducted by the Japan Weather Association and a flight test using the Japan Aerospace Exploration Agency's research helicopter MuPAL-ε, which is equipped with a novel ultrasonic velocimeter instrument which enables measurement of winds with 2kt accuracy and 1m spatial resolution. In the flight test, MuPAL-ε flew around and over the planned heliport site to acquire wind data, and performed takeoffs and landings to evaluate the effects of cliff-top turbulence on flight safety. The results are summarized as follows: 1) MuPAL-ε successfully measured cliff-top turbulence in westerly wind conditions, when the heliport site is in the lee of an especially steep cliff face, and revealed its detailed structure. 2) CFD analysis using a k-ε turbulence model clarified the general characteristics of the local wind field under various prevailing wind speeds and directions. However, comparison with flight test results revealed that the k-ε turbulence model cannot predict the cliff-top turbulence structure in detach regions, and so another turbulence model, such as Large Eddy Simulation, is needed. 3) Helicopter responses to cliff-top turbulence were evaluated in 20–40kt westerly wind conditions in which strong turbulence is likely to occur. The evaluation results indicate that operational wind limits are needed for westerly winds to ensure the safety of operations at the planned heliport.

Introduction

Helicopters may occasionally encounter atmospheric turbulence with very small spatial scales, especially during rescue operations in mountainous areas or when carrying out roof-top takeoffs and landings. Large, abrupt changes in wind speed and direction cause attitude fluctuation and height loss. Although the effects of localized turbulence on helicopter flight are critical, no safety criteria have been established, nor has the structure of such turbulence been fully clarified. While numerical analysis using a computational fluid dynamics (CFD) is widely used to investigate such small-scale turbulence, field measurement data are needed to verify the CFD codes, but existing wind observation systems such as GPS sonde or Doppler sodar/radar/lidar lack sufficient accuracy, response, and spatial resolution to clarify the structure of small-scale turbulence.

The Japan Aerospace Exploration Agency (JAXA) has been studying the use of aircraft to measure atmospheric turbulence. JAXA's research helicopter MuPAL-ε (Fig 1, Refs 1, 2), based on an MH2000A (Ref 3), is equipped with a novel turbulence sensor that measures

Fig 1 JAXA's Research Helicopter MuPAL-ε.

atmospheric turbulence with high accuracy and at high temporal/spatial resolutions, sufficient for observations of small-scale turbulence to verify CFD results. MuPAL-ε is also equipped with a data acquisition system that provides extensive flight data, such as inertial data, main rotor status and engine parameters, allowing the gust response of the helicopter to be evaluated concurrently with wind measurement.

This paper describes the measurement and evaluation of cliff-top turbulence for the qualification of a planned heliport at Aogashima Island. Aogashima Island (Fig 2) is located 350km south of Tokyo, and its inhabitants use a commuter helicopter for daily transportation to and from another island. To avoid mists during the rainy season, Aogashima village has planned a new heliport on a small flat area in the northernmost part of the island, at an elevation of approximately 200m above mean sea level (MSL), lower than current heliport (Fig 1, 270m MSL). However, as Fig 2 shows, the planned heliport site is surrounded by steep cliffs that may cause strong turbulence, thus compromising flight safety on windy days. Figure 3 illustrates the track of a balloon released from the cliff-top in a 20kt westerly wind. The complicated track shows the existence of strong turbulence over the cliff-top surface. The Aogashima village administration therefore contracted Toho Air Service Co., Ltd., which operates the local commuter helicopter, to carry out a feasibility study of the planned heliport including an investigation of the local wind field. JAXA and the Japan Weather Association (JWA) participated in the wind field investigation by carrying out flight tests using MuPAL-ε and a CFD analysis, respectively.

Fig 2 Aogashima Island Heliports.

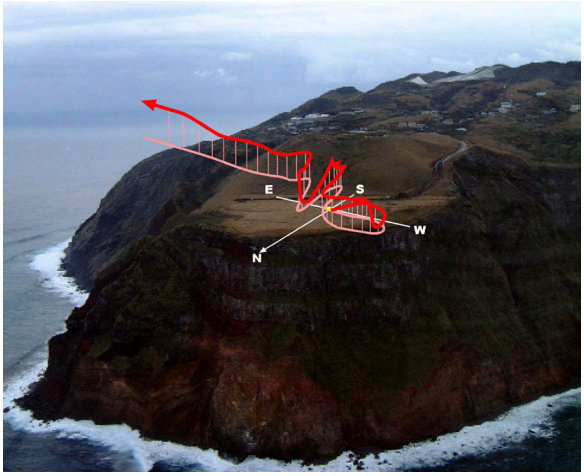

Fig 3 Balloon Track in a 20kt Westerly Wind.

This paper is structured in three main sections. First, the wind measurement capability of MuPAL-ε and its novel turbulence sensor are described. Second, the results of CFD analysis and the flight test are presented. The structure of cliff-top turbulence is clarified and some shortcomings of the CFD analysis are revealed through comparison with the flight test results. Third, helicopter response to cliff-top turbulence is evaluated, with inertial data and main rotor status of MuPAL-ε during encounters with cliff-top turbulence presented.

Wind Measurement Capability of MuPAL-ε

MuPAL-ε onboard sensors

Wind is obtained by subtracting airspeed from ground speed, with compensation for aircraft angular motion. Ground speed and angular velocity data are provided by an onboard DGPS/INS (Differential Global Positioning System/Inertial Navigation System) with respective accuracies of 0.2kt and 0.1deg/sec. Airspeed data are provided by a conventional airdata boom or a novel air data sensor called an ultrasonic velocimeter (USV, Fig 4), which is based on an ultrasonic anemometer commonly used in meteorological observation. The USV has a great advantage as a turbulence sensor in that it can measure 3-axis airspeeds with 0.5kt

accuracy at a high sampling rate (20Hz) even in low speed regions where a Pitôt-static system is ineffective. The major difference between the USV and ordinary ultrasonic anemometers is the probe shape; the shape of the USV probe has been modified to suppress sonic noise at high speed so that it can be used over the entire helicopter flight speed range.

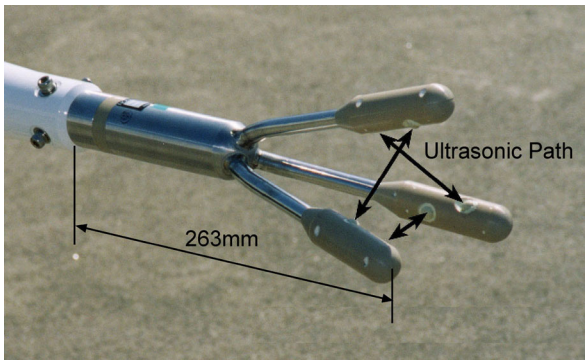

Fig 4 USV Probe.

Position Error Correction

The main error source of wind measurement from a flight vehicle is the position error at the location of the air data sensor, i.e. the effects of the flow around the fuselage and the rotor wake. To minimize position error even in low speed flight, the USV is installed at the tip of an extended nose boom (Fig 5), about 1m ahead of main rotor blade tip and 0.6m ahead of an airdata boom which can be installed in place of the USV.

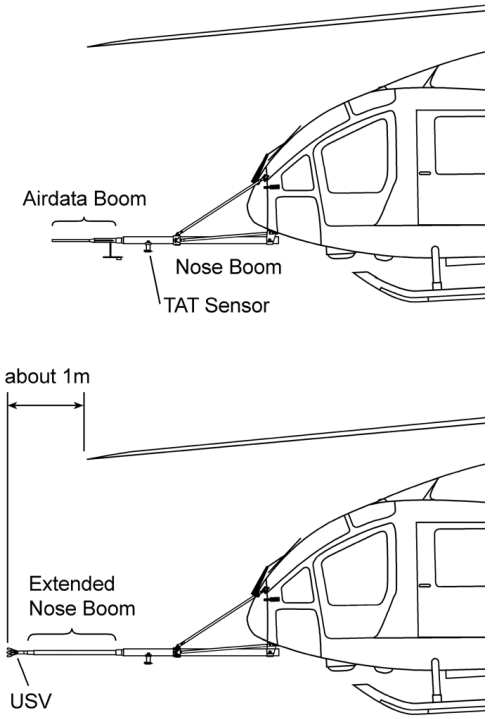

Fig 5 Installed Locations of USV and Airdata Boom.

Extensive flight tests have been conducted to determine the position error. Figure 6 exemplifies the measured position error in steady level flight at the USV and airdata boom locations. The position error of the USV is 3–4kt, smaller than that of the airdata boom. However, even at the USV installed location, the variation of position error significantly increases and become unpredictable at less than 20kt due to the rotor wake.

Reliable airspeed data can therefore be acquired only when airspeed is greater than 20kt. The expected overall wind speed accuracy and spatial resolution at an airspeed of 40kt are 2kt and 1m respectively.

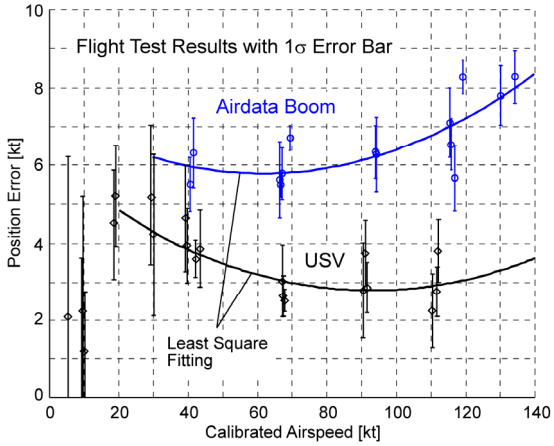

Fig 6 Position Error at USV and Airdata Boom Locations.

Wind Field Evaluation around Planned Cliff-top Heliport

Wind Field Analysis Using CFD

Prior to the wind measurement flight test, JWA performed a CFD analysis to clarify the general characteristics of the local wind field, in particular to identify the conditions in which turbulence is likely to occur. Table 1 summarizes the features of CFD model used in the analysis. The analyzed

cases are shown in Table 2. These cases correspond to the prevailing winds at Aogashima Island during the windy seasons. Two computation grids were used since the prevailing wind direction should be normal to the computation grid. Figure 7 shows the computation grids for northeasterly and southwesterly winds.

Figures 8 and 9 show the turbulent kinetic energy (TKE) calculated by the CFD analysis. Figure 8 compares the TKE with different prevailing wind directions at 30kt wind speed. Strong turbulence at the cliff edge is observed only in northwesterly winds because the cliff face at the west of the heliport site is especially steep. Figure 9 shows the TKE at different altitudes under a 30kt northwesterly wind. The turbulent area is limited to low altitudes, around 30–50m above ground level (AGL). In this paper, AGL is defined as the height above the planned heliport surface, which is at an elevation of 207m MSL.

Figure 10 shows horizontal and vertical wind speed distributions. The cliffs cause the horizontal wind speed to increase by 5–10kt, and

Table 1 CFD Model Used in the Wind Field Analysis.

Governing Equation	3-D Navier- Stokes
Turbulence Model	k-ε Model
Discretization Method	Finite Volume Method
Differencing Schemes	QUICK (Third Order)
Grid Coordinates	Boundary-Fitted Curvilinear Coordinates
Computation Region	2km x 2km (Horizontal) x 2km (Vertical)
Computation Grids	69 x 69 (Horizontal) x 30 (Vertical)
Grid Spacing	10-50m

Table 2 CFD Analysis Cases.

Wind Direction [deg]	60	240	310
Wind Speed [kt]	30, 40	30, 40	30, 40, 50

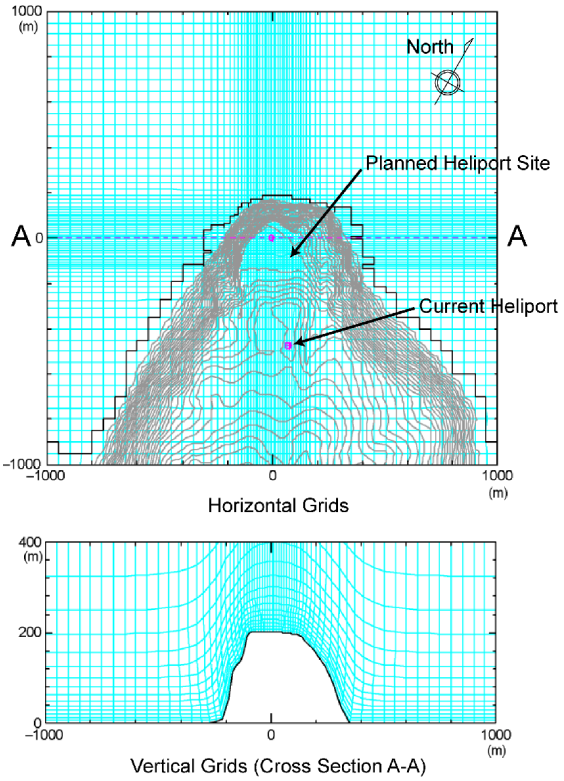

Fig 7 Computation Grid for Northeasterly and Southwesterly Winds.

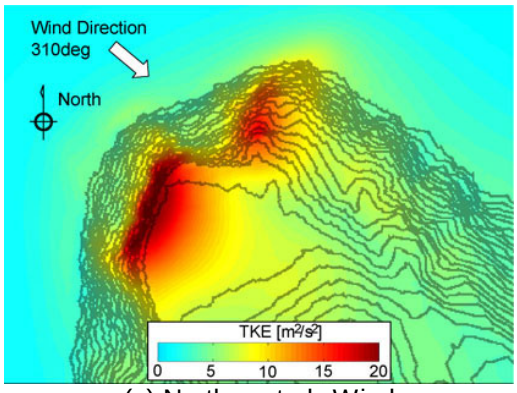

(a) Northwesterly Wind

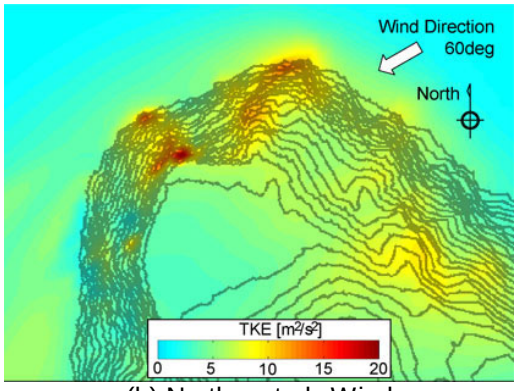

(b) Northeasterly Wind

Fig 8 Turbulent Kinetic Energy at Different Prevailing Wind Directions. (Wind Speed 30kt)

a 20kt upwash is produced at the windward cliff edge. On the other hand, a 10kt downwash is observed at the leeward cliff edge.

These CFD analysis results indicate that strong turbulence is likely to occur at the windward cliff edge in northwesterly winds. Considering this, the flight tests were conducted mainly in northwesterly wind conditions.

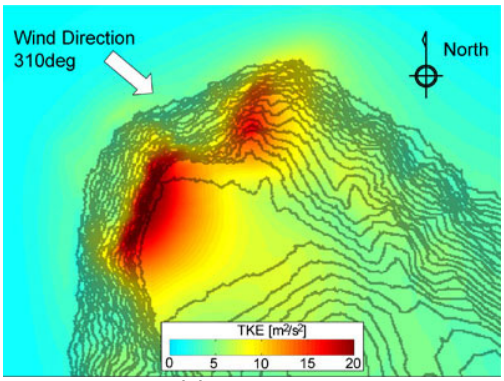

(a) 30m AGL

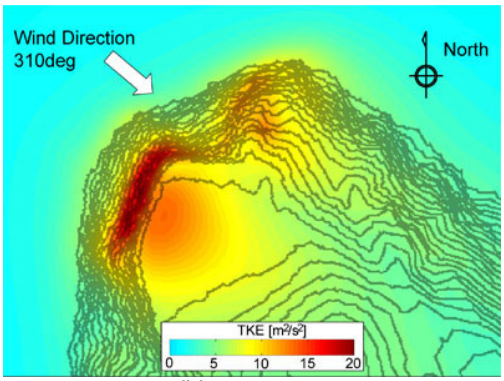

(b) 50m AGL

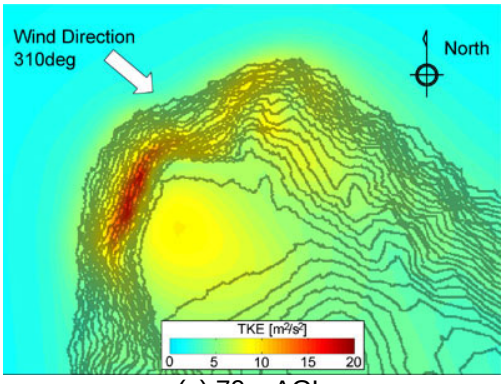

(c) 70m AGL

Fig 9 Turbulent Kinetic Energy at Different Heights AGL. (Wind Direction 310degrees, Wind Speed 30kt)

Wind Measurement Flight Test

Figure 11 illustrates the wind measurement flight patterns, which were flown at 15–70m AGL. A flight speed of 70kt was selected to maximize excess engine power for flight safety and ensure wind measurement accuracy. The objective of patterns A1 and A2 was to investigate the wind field over the planned heliport site at different heights AGL, and patterns B and C were intended to investigate upwash and downwash at

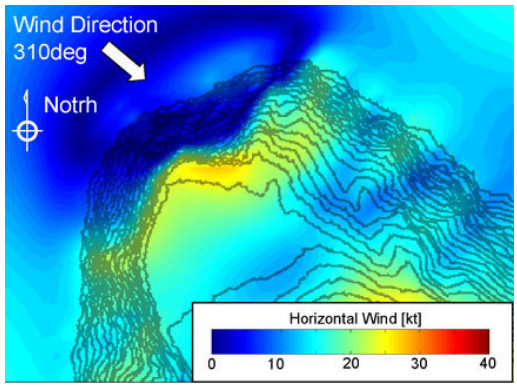

(a) Horizontal Wind Speed

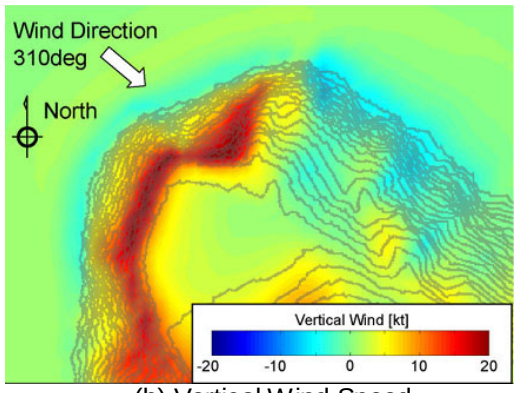

(b) Vertical Wind Speed

Fig 10 Horizontal and Vertical Wind Speed Distributions. (Wind Direction 310degrees, Wind Speed 30kt)

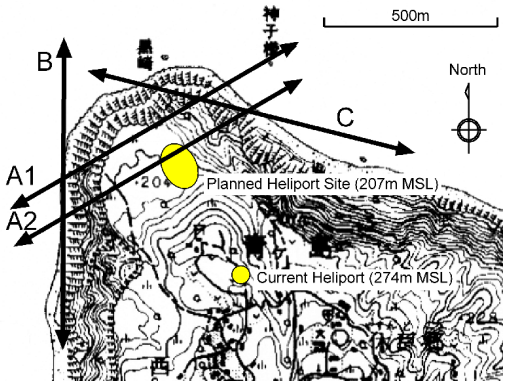

Fig 11 Wind Measurement Flight Patterns.

the cliff edges. The helicopter's precise position derived from the onboard DGPS/INS and the prescribed flight paths were indicated to the pilot on a programmable cockpit display (Fig 12). To ensure flight safety, the flight test was started from high AGL patterns and proceeded to lower AGL patterns when the safety at the high AGL patterns was confirmed.

Figures 13 and 14 show the measured winds around the planned heliport site under two different prevailing wind conditions. The prevailing wind conditions of Fig 13 are north-northeasterly winds of 10–15kt, and those of Fig 14 are northwesterly winds of 20–30kt. The observed results are summarized as follows: 1) Turbulence over the planned heliport site was stronger in a westerly wind than in an easterly wind. 2) Turbulence was observed mainly at 40m AGL or below. At 70m AGL, no turbulence was observed. 3) A 5–20kt (≅ 500–2000fpm) upwash was observed at the windward cliff edge and a 5–10kt (≅ 500–1000fpm) downwash was observed at leeward cliff edge. 4) In northwesterly wind conditions (Fig 14), the wind speed decreases dramatically over the planned heliport site below 40m AGL, and a 10kt (≅ 1000fpm) upwash/downwash was also observed.

Figure 15 exemplifies strong cliff-top turbulence measured by flight pattern A2 flown at 30m AGL in strong westerly winds. Horizontal wind speed increased up to 50kt at the windward cliff edge and then abruptly decreased to under 5kt over the cliff top. Wind direction also fluctuated greatly, even becoming opposite to the prevailing wind. At the same time, the variation of vertical wind speed reached ±20kt, and peak downwash was greater than 25kt.

Comparison of Turbulence Structure between Flight Test and CFD Analysis

The flight test results agree well with the CFD analysis results and indicate that the CFD analysis provides an accurate picture of the general characteristics of the local wind field. However, some discrepancies are also observed between the calculated and measured local turbulence over the planned heliport site. Here, the measured turbulence data, obtained by flight patterns A1 and A2 at around 30m AGL, are compared with the CFD results. Table 3 shows the prevailing wind conditions of both the flight test and the CFD analysis. Although the wind directions are almost the same, the wind speed measured during the flight test is less than that of the CFD analysis.

Table 3 Prevailing Wind Conditions of Flight Test and CFD Analysis Used in Figs 16, 17.

	CFD	Flight Test
Wind Direction [deg]	310	297-307
Wind Speed [kt]	30	20-23

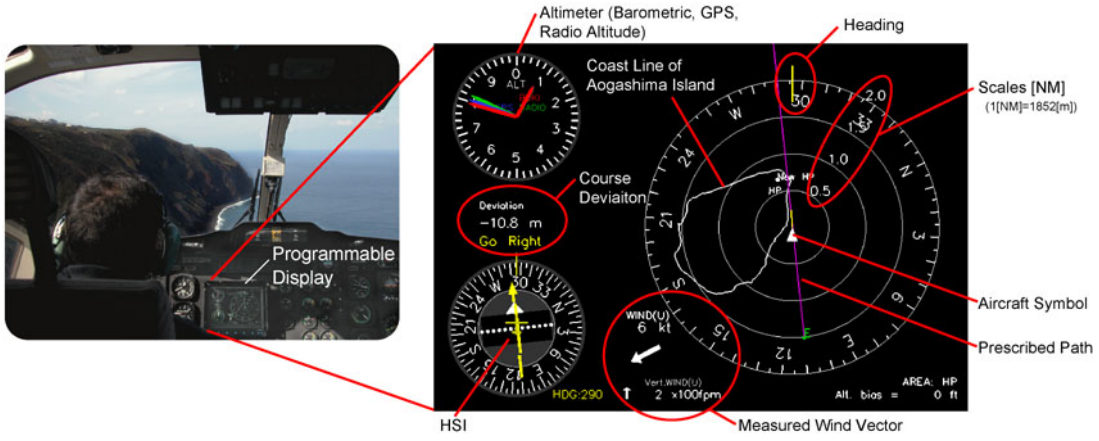

Fig 12 Programmable Cockpit Display.

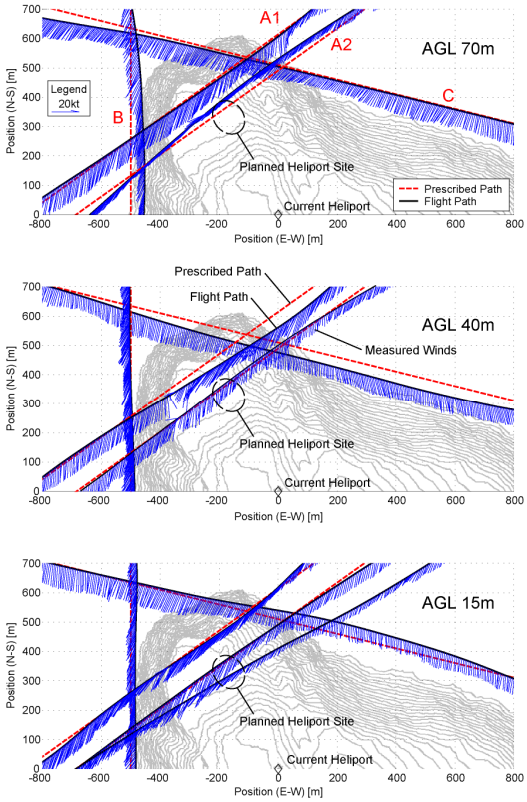

(a) Horizontal Winds at Different Heights AGL.

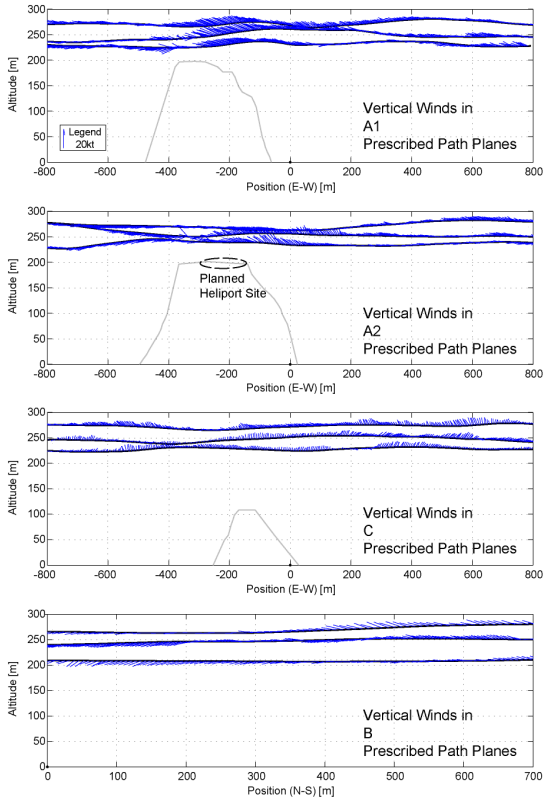

(b) Vertical Winds in Prescribed Path Planes.

Fig 13 Measured Winds. (Wind Direction 10-30 degrees, Wind Speed 10-15kt)

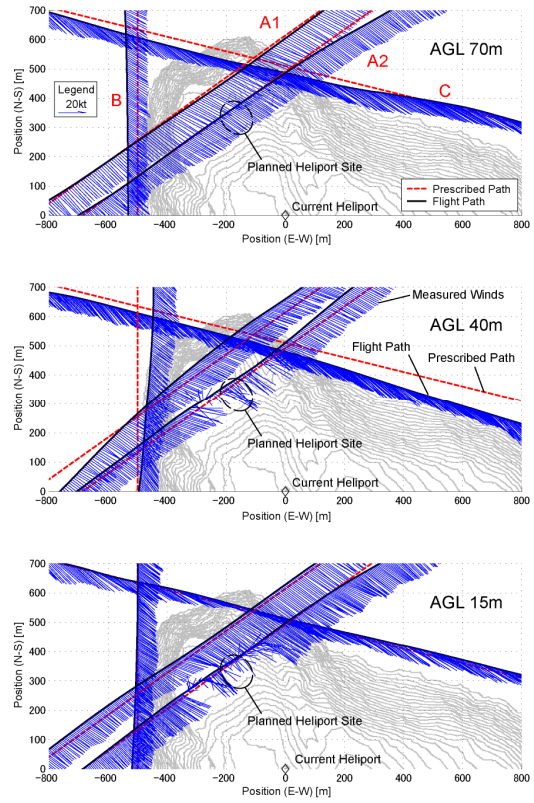

(a) Horizontal Winds at Different Heights AGL.

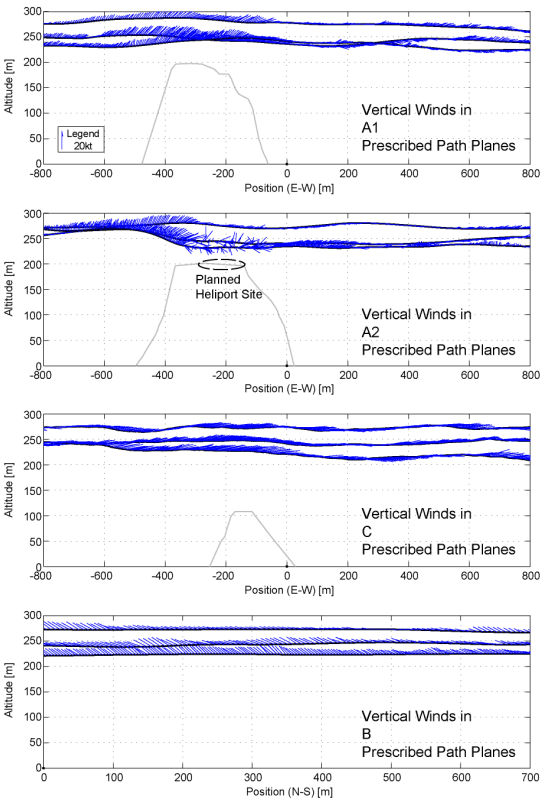

(b) Vertical Winds in Prescribed Path Planes.

Fig 14 Measured Winds. (Wind Direction 300-310 degrees, Wind Speed 20-30kt)

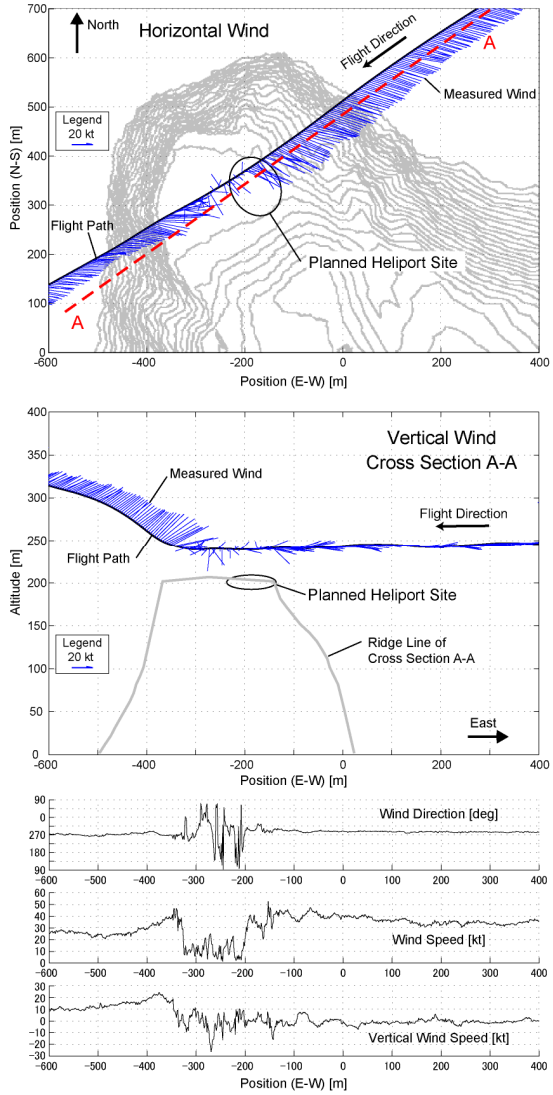

Fig 15 Measured Winds. (Wind Direction 280-290 degrees, Wind Speed 35-40kt)

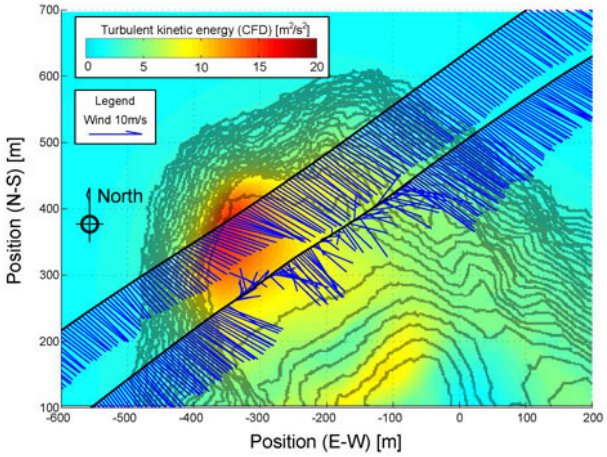

Fig 16 Comparison of Measured Winds and Computed Turbulent Kinetic Energy.

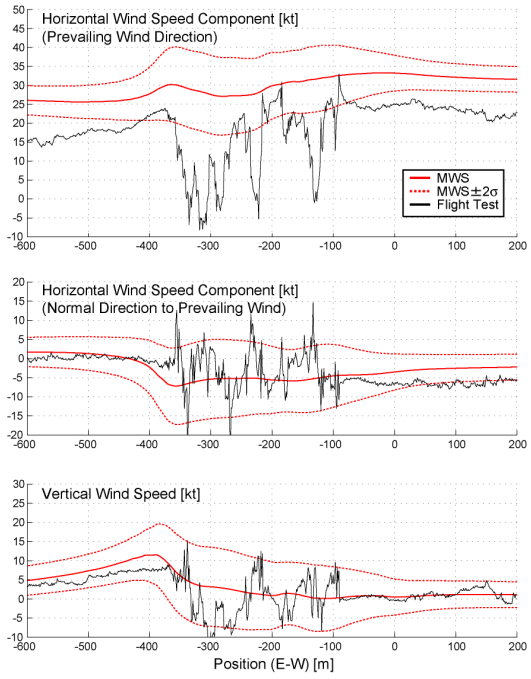

(a) Pattern A2, Run 1

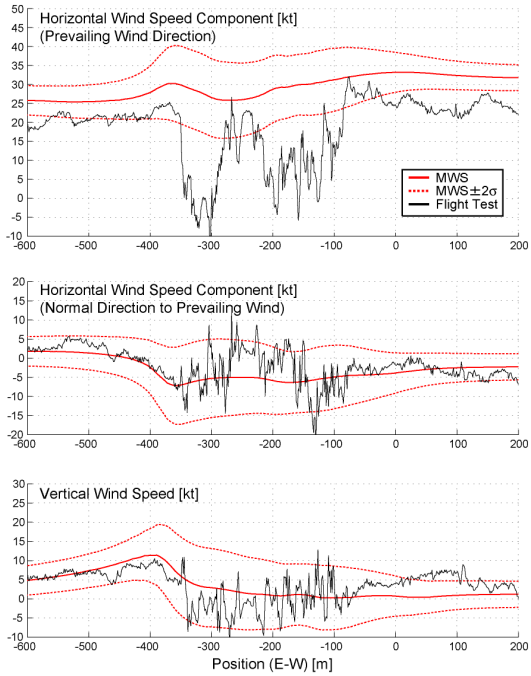

(b) Pattern A2, Run 2

Fig 17 Comparison of Wind Speed Variation between Flight Test and CFD Analysis.

Turbulence Distributions: Figure 16 compares turbulence distributions. The CFD analysis indicates that the strongest turbulence is generated at the windward cliff edge, while the measured turbulence was the most severe over the middle of the cliff top.

Wind Speed Variations: Here, the wind speed variations observed during the flight test are quantitatively compared with the CFD results. However, direct comparison is not feasible, since the flight test data are a series of instantaneous values at spatially and temporally different points, while the CFD analysis results using the k-ε turbulence model are time-invariant statistical values, mean wind speed (MWS) and TKE, at fixed grid points. Since there are not enough flight test data to derive statistical measurements, wind speed data comparable to the flight test data are derived from the CFD analysis results by the following procedure: 1) The CFD analysis results under a 30kt prevailing wind are multiplied by two-thirds to adjust to the flight test condition, a 20kt prevailing wind. This relies on the intuitive assumption that the local wind field structure under a 20kt prevailing wind is similar to that under a 30kt wind. 2) Calculate MWS and TKE along the flight path by linear interpolation of the CFD results at fixed grid points. This assumes that MWS and TKE vary linearly between grid points. 3) Calculate the standard deviation of wind speed (σ) using TKE and the isotropy assumption. 4) Compare the flight test data with MWS and σ.

Figure 17 compares the observed wind speed variations for pattern A2, which was flown twice successively during the flight test, with the MWS and σ values calculated by the above procedures. Except for along the prevailing wind axis, the flight test and the CFD analysis results correspond well; the differences between the flight test data and MWS lie almost entirely within the $\pm 2\sigma$ region. Along the prevailing wind axis, however, the flight test results vary far beyond the $\pm 2\sigma$ region. Although the flight test results include both spatial and temporal variations and it is difficult to distinguish spatial variations from temporal ones, the observed wind speed variations along the prevailing wind axis seem to be mainly spatial variations, since similar variation patterns were observed in two temporally different cases (Fig 17 (a), (b)). This indicates that the CFD analysis does not reproduce the observed drop in MWS over the planned heliport site.

The discrepancies shown here are all occur in a “detach” region (i.e. where the flow separates from the surface), in which the prediction of flow fields is particularly difficult. Some of the discrepancies may be resolved by changing the turbulence model used in the CFD analysis, from the k-ε model to another model such as the Large Eddy Simulation (LES) model.

Evaluation of Helicopter Response to Cliff-top Turbulence

Considering the wind field measurement results, the heliport was planned to be sited at the southeastern end of the cliff top, where the turbulence seems to be relatively weak even in strong westerly winds. A further flight test was conducted using MuPAL-ε to evaluate helicopter operations at this site, with twelve takeoffs and landings performed at the planned site in 20–40kt northwesterly winds. The measured cliff-top turbulence and helicopter responses of typical three cases are shown in Figs 18–20.

Operation at Wind Speeds of 15–25kt

The measured winds are shown in Fig 18(a) and the helicopter responses during landing approach and hovering over the heliport site are presented in Fig 18 (b). Note that the lateral axis of Fig 18 (a) is aircraft position and that of Fig 18 (b) is elapsed time. The flight directions of each figure are opposite; that of Fig 18 (a) is from right to left and that of Fig 18 (b) is from left to right. This is also true for Figs 19 and 20. Wind data were not available during hovering (elapsed time 30–80sec) since the forward airspeed was too slow, below 20kt, to produce reliable data. The observed turbulence was relatively weak; the variations of wind speed over the heliport site

were ±10kt horizontally and ±5kt vertically. During hovering over the heliport site, no significant attitude disturbance was observed and the amplitude of the fluctuation of vertical acceleration was ±0.1G. The pilot felt that there was sufficient excess engine power to be able to respond to downwash, since the observed vertical wind speed variation was small. Consequently, operations at this wind condition seemed to be acceptable.

Operation at Wind Speeds of 25–35kt

The measured winds are shown in Fig 19(a), a more severe condition than the previous case. The helicopter responses during landing approach, short duration hover over the heliport site and take-off to the north are shown in Fig 19 (b). The horizontal wind speed rapidly decreased over the heliport site from over 30kt to under 10kt, while vertical wind speed varied over ±15kt. Hovering over the heliport site, the pilot had to use excessive engine power control up to 110% engine torque to maintain altitude. There was therefore no excess engine power available and so hovering at low altitude was not attempted in this case. The take-off to the north, chosen because wind measurement results indicated that turbulence is relatively weak at the north cliff-edge, was found to be effective since the time spent in the turbulent region was shorter than for take-offs to the west.

Operation at Wind Speeds of 35–40kt

The measured winds are shown in Fig 20(a),

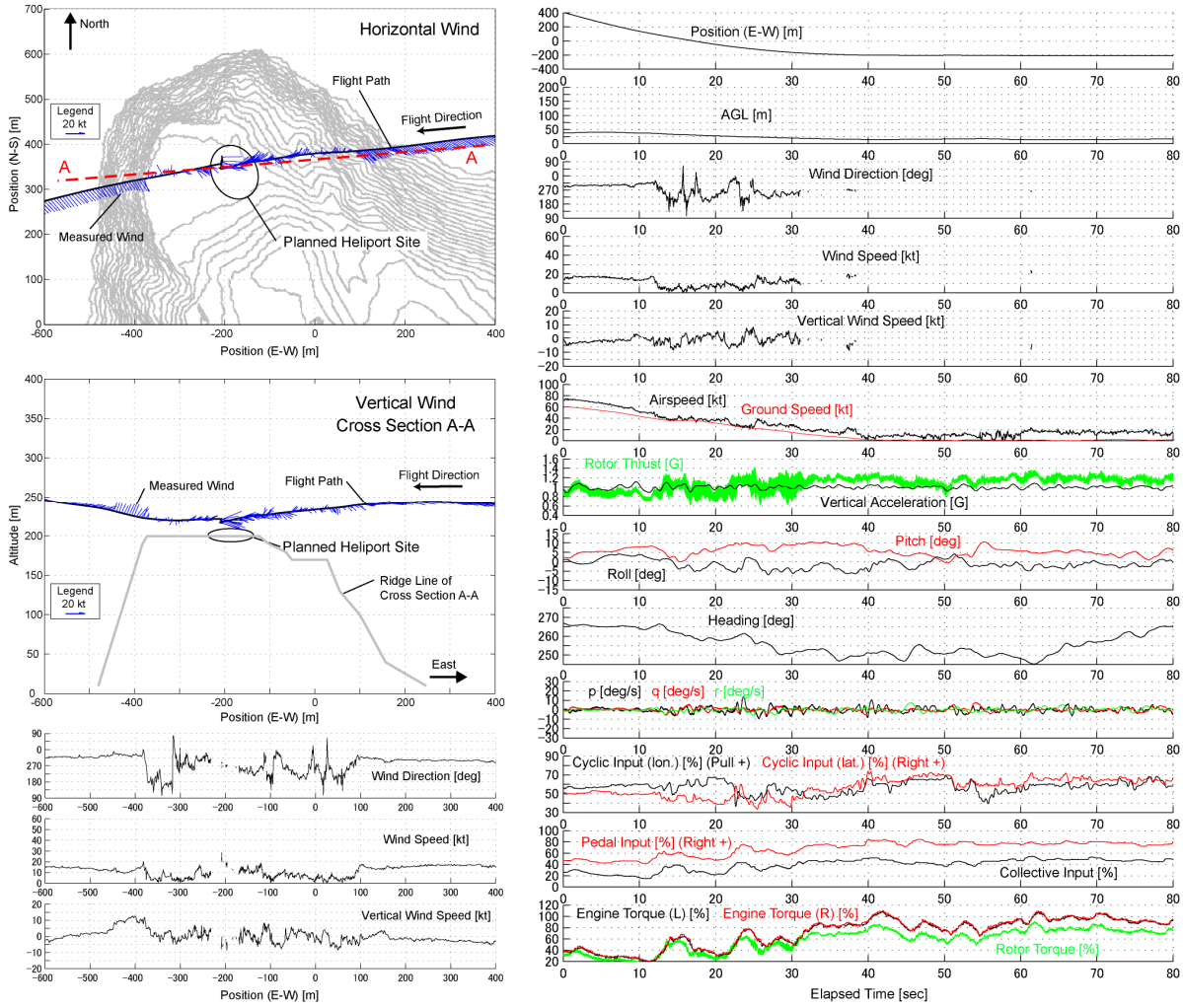

(a) Measured Winds. (b) Time Histories of Helicopter Response.

Fig 18 Measured Winds and Helicopter Response.
(Wind Direction 310-320 degrees, Wind Speed 15-25kt)

which is the severest condition among the flight test cases and possible nearly 5% of the time throughout the year. In this case, the pilot abandoned hovering over the heliport site due to strong cliff-top turbulence. The helicopter responses during landing approach and low pass over the heliport site are shown in Fig 20 (b). Although the pilot tried to maintain airspeed at 70–80kt during approach, the airspeed fell abruptly to under 20kt when flying over the heliport site because a nearly 40kt head wind suddenly disappeared there. Vertical wind variation of over 20kt (≅ 2000fpm) was also observed, and this variation caused significant fluctuation of rotor thrust, which led to vertical acceleration varying over a peak-to-peak range of almost 1G. Aircraft attitude was also affected by gusts, with 15–20 degrees changes of roll and heading angles being observed.

Figure 21 shows the time histories of the six components of main rotor force (Fx, Fy, Fz) and moment (Mx, My, Mz), and flapping angle of the main rotor blades (β) and its Fourier series coefficients (β_0, β_c, β_s), over the same time periods as Fig 20 (b). The forces and moments were measured by strain gages attached to the rotor shaft (dynamic mast), and the flapping angles were measured by small plates with strain gages installed in the blade hinges. The forces and moments in Fig 21 are expressed in a body-fixed axis system and the flapping angle is expressed in a shaft axis system. Rotor thrust (Fz) varied with vertical wind variation and its

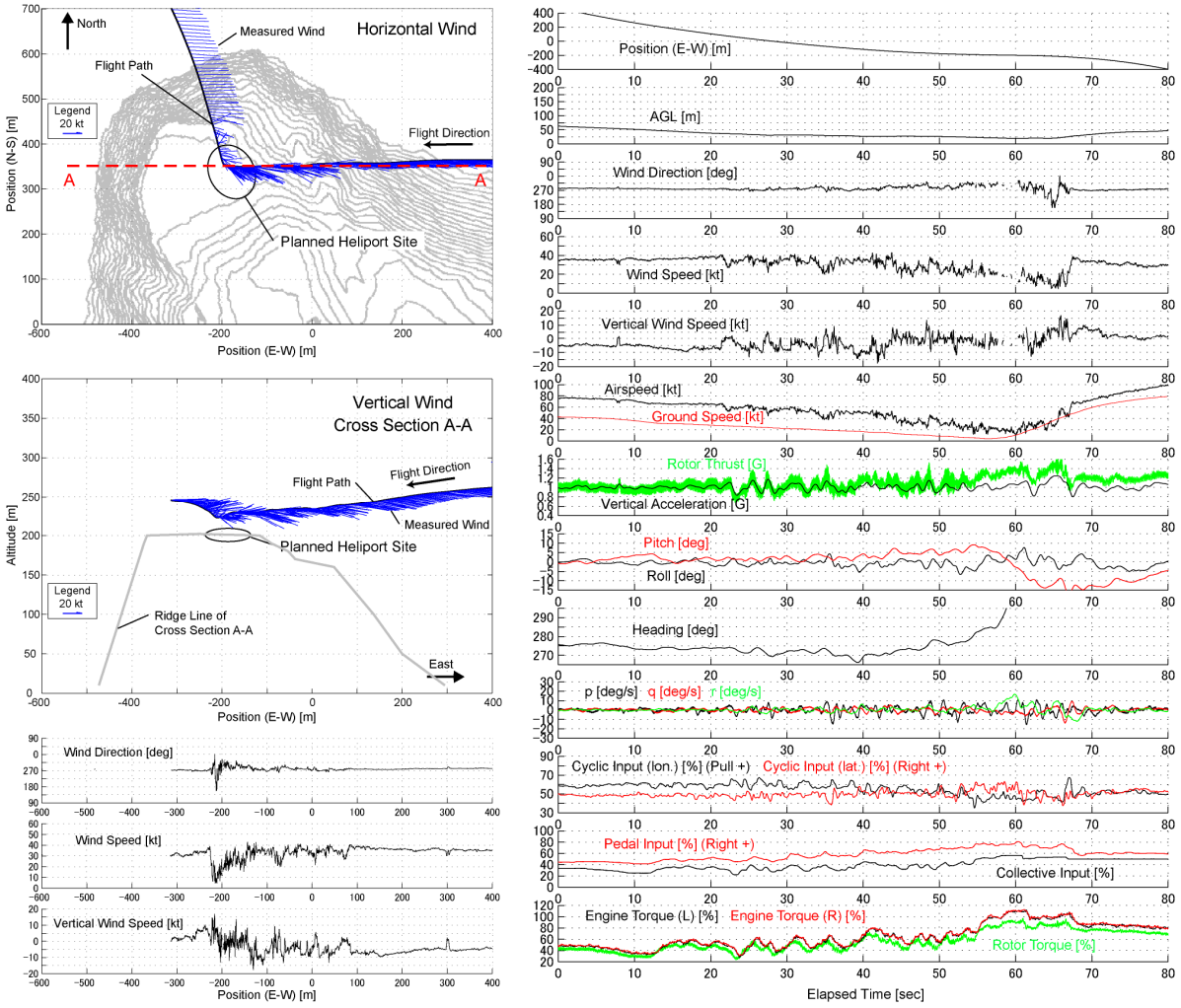

(a) Measured Winds. (b) Time Histories of Helicopter Response.

Fig 19 Measured Winds and Helicopter Response.
(Wind Direction 280-290 degrees, Wind Speed 25-35kt)

peak-to-peak range reached 40kN, almost the same as MuPAL-ε's weight (4200kg). Relatively large rolling (Mx) and pitching (My) moments were also observed. For example, a ±4kN•m rolling moment observed at 35sec elapsed time corresponds to an angular acceleration of ±60deg/s^2. As well as rotor forces and moments, β_0, β_c, and β_s mainly varied with vertical wind variation with an amplitude of ±2–3degrees.

Wind Limits for Heliport Operation

The evaluation flight test results indicate that wind limits are needed under westerly prevailing wind conditions to ensure the safety of operations at the planned heliport. The wind speed limit is supposed to be below 30kt, which is possible nearly 10% of the time throughout the year in this area.

Conclusions and Future Plans

Conclusions

This paper has described the measurement and evaluation of cliff-top turbulence for the qualification of a planned heliport. The evaluation method, which utilizes CFD analysis to determine which wind conditions are likely to be critical and flight tests to obtain detailed data on such conditions, worked quite well. The obtained results are summarized as follows:

1. MuPAL-ε successfully measured cliff-top turbulence in westerly wind conditions and revealed its detailed structure.

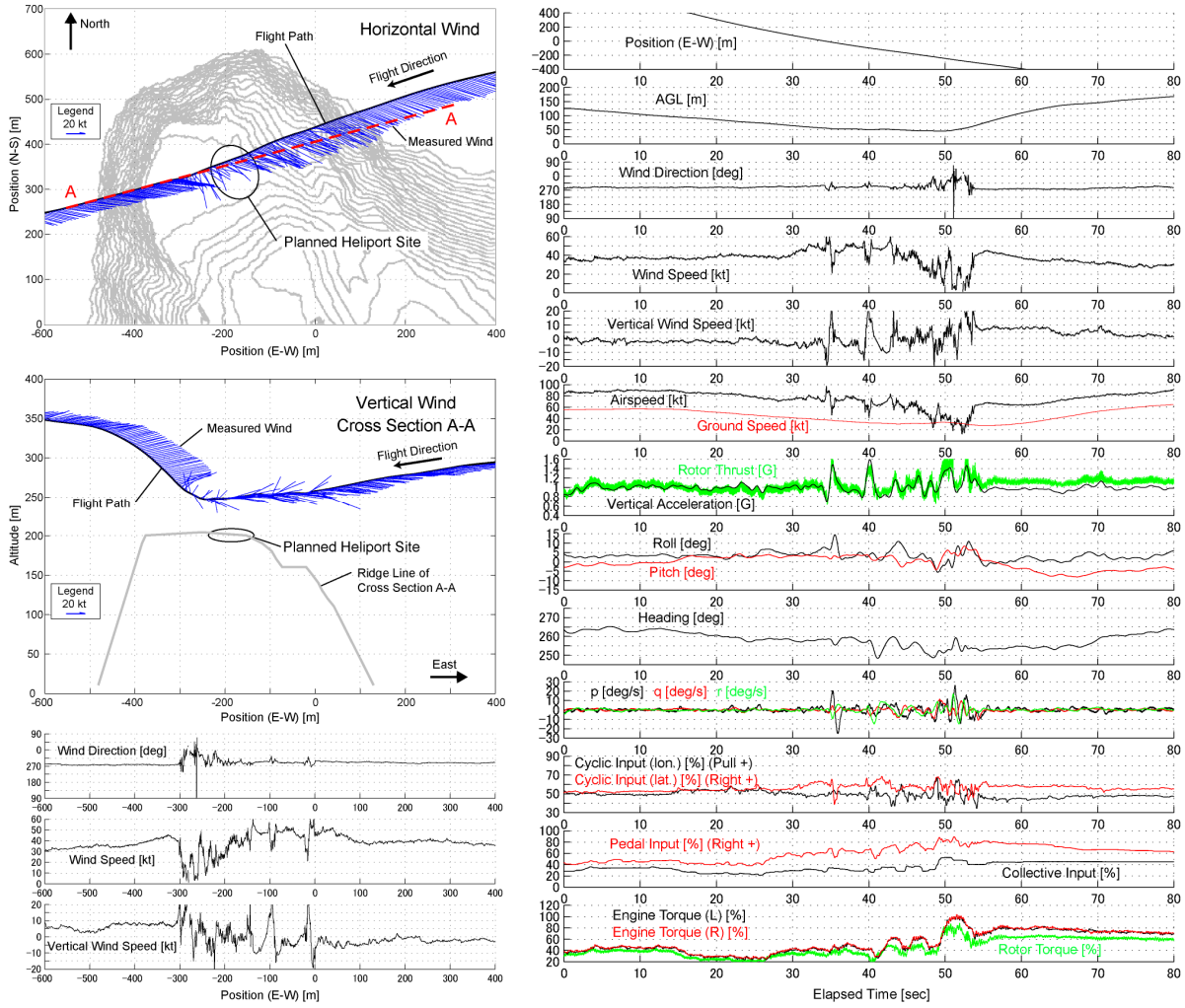

(a) Measured Winds. (b) Time Histories of Helicopter Response.

Fig 20 Measured Winds and Helicopter Response.
(Wind Direction 280-290 degrees, Wind Speed 35-40kt)

2. CFD analysis using the k-ε turbulence model clarified the general characteristics of the local wind field under various combinations of prevailing wind speed and direction. However, comparison with the flight test results revealed that the k-ε turbulence model cannot predict the structure of the cliff-top turbulence in detach regions.
3. Helicopter responses to cliff-top turbulence were evaluated in 20–40kt westerly wind conditions. The evaluation results indicate that wind limits need to be imposed for operations in westerly winds to ensure the safety of flight operations at the planned heliport.

Future Plans

Another CFD program based on an LES model is currently being developed by the Tokyo Institute of Technology. Development of an atmospheric turbulence model for a flight simulator (Fig 22) is also ongoing to evaluate the wind limits at this heliport.

Acknowledgements

The authors would like to express sincere thanks to all those who provided their help and advice for this flight test, especially to the residents of Aogashima Island.

References

1. Okuno, Y., and Matayoshi, N., Development of a New Research Helicopter MuPAL-ε, AHS 57th Annual Forum Proceedings, Washington, D.C., May 2001.
2. Okuno, Y., Matayoshi, N., and Ishii, H., Recent Research Programs of the MuPAL-ε Research Helicopter, 24th ICAS, Yokohama, Japan, 29 Aug-3 Sep 2004.
3. Kobayashi, T., and Sakura, K., Development of MH2000, New Commercial Helicopter, AHS 56th Annual Forum Proceedings, Virginia, May 2000.

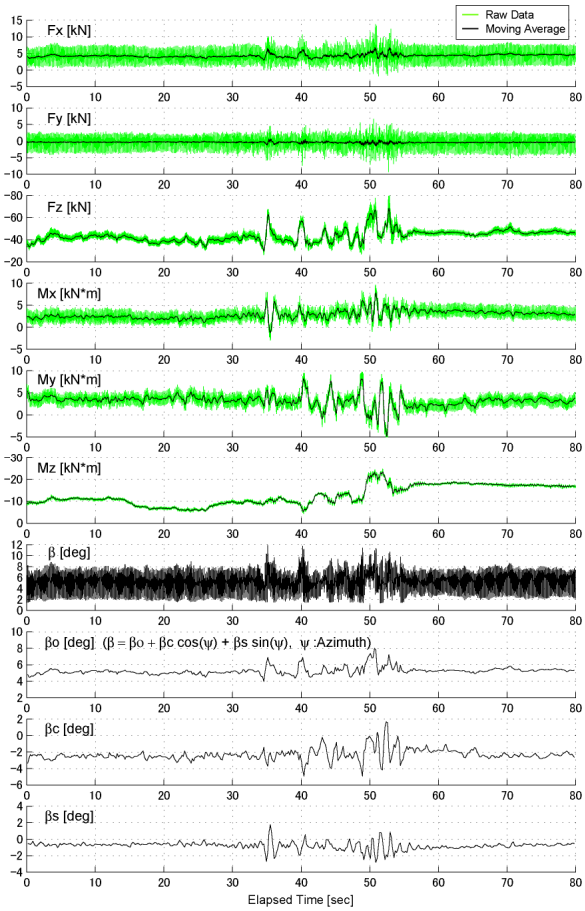

Fig 21 Time Histories of Main Rotor Forces/Moments and Blade Flapping.
(Wind Direction 280-290 degrees, Wind Speed 35-40kt)

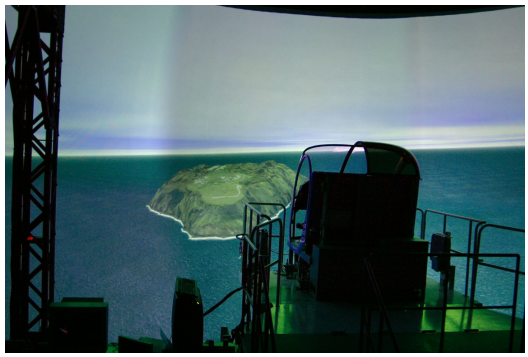

Fig 22 Setup of Helicopter Flight Simulator.